One-Layer Rate-Splitting Multiple Access with Benefits over Power-Domain NOMA in Indoor Multi-cell Visible Light Communication Networks

Siyu Tao†, Hongyi Yu*†, Qing Li†, Yanqun Tang‡, Di Zhang§
†National Digital Switching System Engineering and Technological Research Center (NDSC), Zhengzhou, China
‡ School of Electronics and Communication Engineering, Sun Yat-sen University, Guangzhou, China
§ School of Information Engineering, Zhengzhou University, Zhengzhou, China
Email: peachforworking@foxmail.com, xxgcmaxyu@163.com*, liqing0206@163.com,
tangyq8@mail.sysu.edu.cn, dr.di.zhang@ieee.org

***Abstract*—A conventional approach to tackle the inter-cell interference in multi-cell visible light communication (VLC) networks is based on non-orthogonal multiple access (NOMA) by allowing one user to fully decode the message of another user. Due to the ability of partially decoding the interference and partially treating it as noise, rate-splitting multiple access (RSMA) has been regarded as a more flexible interference management scheme that generalizes and outperforms NOMA. Motivated by the benefits of RSMA and its infancy in multi-cell VLC networks, this paper firstly introduces 1-layer RSMA into multi-cell VLC networks by considering the Lambertian radiation model of indoor visible-light channels. Afterwards, we develop a linear precoding containing 1-layer RSMA-VLC to achieve spectral efficiency having constrained the non-linear effect of a light-emitting diode (LED). Subsequently, the transmitted power allocation is constrained by the optical signal power. Finally, we perform a comparison between 1-layer RSMA and NOMA based on multi-cell VLC networks. Simulation results show the effectiveness of our proposal in system spectral efficiency and VLC constraints. Furthermore, key features guaranteeing the merits of 1-layer RSMA are analysed with respect to the number of users, user locations, and lighting deployment.**

***Index Terms*—visible light communication, rate-splitting multiple access, non-orthogonal multiple access, spectral efficiency, lighting deployment**

I. Introduction

Visible light communication (VLC) is an optical wireless communication technology utilizing light-emitting diodes (LEDs) to propagate the radio wave within the visible-light spectrum. However, on the one hand, the limitation of the circuit technology and non-linear effects of LED cause the narrow modulation bandwidth [1]–[3] of common commercial illuminants, which reduces the spectral efficiency. On the other hand, the common modulation scheme adopts intensity modulated and direct detection (IM/DD), which means that the visible-light signal is non-negative and real-valued [4], [5]. In addition, for an optical wireless network, a visible-light signal is highly directional [1], [6], [7]. Although indoor visible light is not subjected to fast fading effects, it possesses channel correlation and close-in inter-cell interference (ICI), where its coverage is smaller than that of WiFi coverage [6], [7]. In summary, the increasing interest of indoor VLC networks has increased the need for spectral efficiency and unique optical network characteristics.

To deal with these problems, non-orthogonal multiple access (NOMA) [8], [9] is considered as a useful multiple access scheme that enhances spectral efficiency. Previous studies related to NOMA-VLC were based on several main ideas. First, hybrid multiple access methods [10]–[14] including orthogonal multiple access (OMA) and NOMA were applied for ICI elimination. Second, distributed resource managements [10], [14]–[18] such as distributed power allocation and signal design of hybrid NOMA were applied for ICI mitigation. Third, coordinated scheduling and joint processing were applied to multi-cell NOMA-VLC networks [19]–[21]. However, previous studies on NOMA-VLC within multi-cell VLC networks did not handle ICI well for the enhancement of spectral efficiency. Power-domain NOMA (PD-NOMA) requires users to fully decode the messages of users with priority order. It is not only difficult to authentically perform interference elimination in hybrid NOMA schemes, but also other aforementioned studies inflexibly combined visible-light interference management approaches with NOMA. Thus, to solve these problems, we hereby introduce rate-splitting multiple access (RSMA) into multiple-cell VLC networks in this paper.

RSMA relies on linearly precoded rate-splitting (RS) with successive interference cancellation (SIC) to decode a part of the interference and treat the remaining part of the interference as noise. As a powerful and flexible spectral efficient strategy, RSMA is an adaptable interference management that contains NOMA and space division multiple access as special cases [22], [23]. References [24], [25] summarized a number of recent RSMA works in the multiple-input single-output (MISO) broadcast channel (BC) with partial channel state information at the transmitter (CSIT) [26]–[28] and perfect CSIT [22], [29], massive multiple-input multiple-output (MIMO) [30], [31], millimeter-wave systems [32], [33], multi-group multicasting [34], [35], coordinated multi-point joint transmission [36], cloud radio access networks [37], simultaneous wireless information and power transfer [38], and cooperative RS in

978-1-7281-7440-2/20/$31.00 ©2020 IEEE

MISO BC with user relaying [25], [39]. To the best knowledge of the authors, little antecedent work has been carried out on RSMA-VLC.

In multi-cell VLC networks, the merits of applying RSMA are indicated as follows. For handling visible-light channels in small coverage, RSMA may flexibly relieve the channel correlation and interference from ICI to improve the spectral efficiency. For reducing SIC complexity, 1-layer RS framework efficiently exploits the existing per capita SIC-receiver architecture, whereas multi-cell NOMA-VLC networks may increase the complexity of SIC. Moreover, as the visible light is modulated by intensity, the complexity of RS framework is intrinsically reduced. For signal splitting, visible light is used for both illumination and communication, while we can properly exploit RS framework to adjust system throughput and illumination intensity. Considering that the line-of-sight (LOS) link is dominative in the indoor environment, we introduce the RSMA into indoor multi-cell VLC networks and investigate its merits from a spectrum efficiency perspective.

In this study, we develop 1-layer RSMA based on indoor visible-light channels, which can maximize the system spectral efficiency in visible-light constraints. First, we introduce 1-layer RSMA framework into the multi-cell VLC networks. Second, based on the Lambertian model of visible-light channels, the linear precoding is formulated to achieve enhanced spectral efficiency considering the constraint of the electric current range of LEDs, which guarantees both illumination and communication. Subsequently, the power allocation of the transmitted signal power is subjected to the constraint of optical power. Finally, after a comparative analysis between 1-layer RSMA and a NOMA benchmark, we captured the phenomenon that the constraints of visible-light channels limit the linear precoding of RSMA, and the performance of RSMA is involved with visible-light channel model. When visible-light channel model is based on Lambertian radiation and the distribution of users is uniform, 1-layer RSMA with the rigorous restrictions of visible-light channels can guarantee the aggregate advantage in the system spectral efficiency.

II. Indoor VLC Channel Model

For indoor multi-cell VLC networks, visible-light channel models commonly rely on the Lambertian radiation assumption [40], where line of sight (LOS) propagation mainly exists in Lambertian radiation. The coverage of a single LED at the ceiling of a room is defined as a cell of VLC network and also called as an attocell [7].

Let us assume that there are N_t LEDs and N_r single-photodiode users, and the channel gain matrix is defined as $\boldsymbol{h}$, where $\boldsymbol{h} \in \mathbb{R}^{N_t \times N_r}$. If we focus on a channel path from an LED to a user in Fig. 1, indoor visible-light channel gain for the LOS path of the k-th user is given by (1).

$$h_k = \frac{(m+1)\,A}{2\pi d_k^2} \cdot \cos^m(\phi_k) \cdot T_f \cdot r_{oe} \cdot g(\psi_k) \cdot \cos(\psi_k), \quad (1)$$

where m is the order of Lambertian emission, A is the detector physical area, d_k is the distance between an LED transmitter and a receiver of the k-th user, ϕ_k is the angle of irradiance of the k-th user, ψ_k is the angle of incidence of the k-th user, T_f is the optical filter gain constant, r_{oe} is optical-electrical conversion efficiency constant, and $g(\psi_k)$ is the optical concentrator gain of the k-th user.

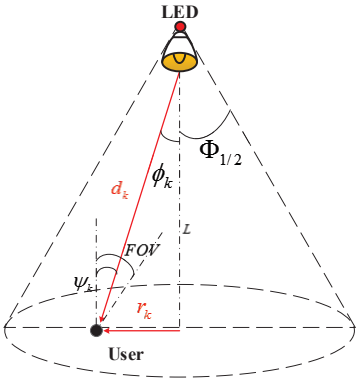

Fig. 1. Lambertian radiation model.

In addition, m and $g(\psi_k)$ can be obtained through (2) and (3), respectively. In the equations, $\Phi_{1/2}$ is the half-power semi-angle of the LED, Ψ_{FOV} is the width of the angle field of vision (FOV) at the receiver, and n_{re} is the refractive index constant.

$$m = -\frac{1}{\log_2\left(\cos\left(\Phi_{1/2}\right)\right)}. \quad (2)$$

$$g(\psi_k) = \begin{cases} \frac{{n_{re}}^2}{\sin^2(\Psi_{FOV})} & ,0 \le \psi_k \le \Psi_{FOV} \\ 0 & ,\psi_k > \Psi_{FOV} \end{cases}. \quad (3)$$

III. 1-Layer RSMA VLC Model

A. 1-Layer RSMA

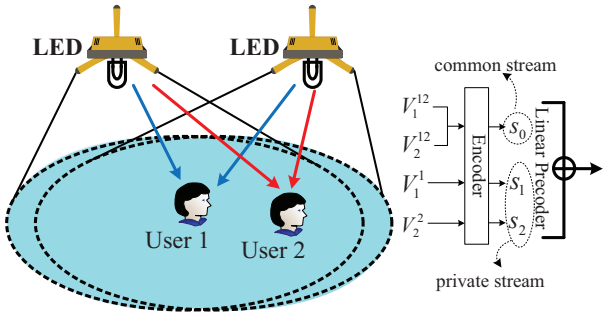

Fig. 2. Two-user example with 1-layer RSMA.

Let us assume that N_t LEDs serve N_r single-photodiode users, and the users are indexed by the set $\mathcal{K} = \{1, \ldots, N_r\}$. The messages $V_1, \cdots, V_{N_r}$ are for user 1 to N_r, and the message of each user in 1-layer RSMA is split into two parts, i.e., $\left\{V_k^{\mathcal{K}}, V_k^k\right\}, \forall k \in \mathcal{K}$. According to the basic concept of the 1-layer RSMA [22] as in Fig. 2, the messages $\left\{V_k^{\mathcal{K}}\right\}, \forall k \in \mathcal{K}$ are encoded into a common stream intended to be decoded by all users, and the message $\left\{V_k^k\right\}, \forall k \in \mathcal{K}$ is encoded into a

private stream to be decoded by the corresponding user. Hence, each user yields a corresponding private stream, and all users combine a common stream.

The data streams can be indicated as $\boldsymbol{s} = [s^{common}, s_1^{private}, \cdots, s_{N_r}^{private}]^T \triangleq [s_0, s_1, \cdots, s_{N_r}]^T$, where $\boldsymbol{s} \in \mathbb{R}^{(N_r+1)\times 1}$. Then, if the number of users is N_r, the number of 1-layer RSMA streams is $N_r + 1$. Based on N_t LEDs and N_r single-photodiode users, the precoding matrix is $\mathbf{W} = [\boldsymbol{w}_0, \boldsymbol{w}_1, \cdots, \boldsymbol{w}_{N_r}] = [\boldsymbol{\omega}_1, \cdots, \boldsymbol{\omega}_{N_t}]^T$, where $\boldsymbol{\omega}_{N_t}^T \in \mathbb{R}^{1\times(N_r+1)}$. Hence, the transmitted visible-light signal of 1-layer RSMA can be indicated as

$$\boldsymbol{x}_{N_t\times 1} = \mathbf{W}_{N_t\times(N_r+1)}\boldsymbol{s}_{(N_r+1)\times 1} + \boldsymbol{d}_{N_t\times 1}, \tag{4}$$

where 1-layer RSMA yields a split signal set in $\boldsymbol{s}_{(N_r+1)\times 1}$ and the transmitted signal after linearly precoding is $\boldsymbol{x}_{N_t\times 1}$. In addition, owing to the non-negative visible-light signal, a direct current (DC) bias vector $\boldsymbol{d} = [d_1, \cdots, d_{N_t}]^T$ can be added to the transmitted LEDs.

Because the DC component exists, the visible-light signal $\boldsymbol{x}$ is non-negative and the original signal $\boldsymbol{s}$ can be designed in bipolar signals. If visible-light channel gain matrix $\boldsymbol{h}_k \in \mathbb{R}^{N_t\times 1}$ for the k-th user is real-valued and non-negative, the received signal y_k for the k-th user can be indicated using (5), where $\boldsymbol{x}_k$ is the transmitted signal for the k-th user and n_k is the zero-mean Gaussian noise at the k-th user. Note that the noise in optical devices is complex and can be caused by different independent sources. Thus, we consider that the noise introduced after photo-electric conversion in the indoor static scenario [41] is zero-mean Gaussian noise [3], [9], [42].

$$y_k = \boldsymbol{h}_k^T\boldsymbol{x}_k + n_k. \tag{5}$$

In VLC, the DC component carries no data; therefore, it can be removed through alternating current coupling at the receiver. We assume that $\boldsymbol{w}_k, k \in [1, N_r]$ is involved with precoder and $p_0, p_k, k \in [1, N_r]$ are related to the stream power. Hence, the signal-to-interference and noise ratio (SINR) of k-th user decoding the common stream is

$$\gamma_k^{common} = \frac{\left|\boldsymbol{h}_k^T\boldsymbol{w}_0 p_0\right|^2}{\sum_{i=1}^{N_r}\left|\boldsymbol{h}_k^T\boldsymbol{w}_i p_i\right|^2 + \sigma^2}, \tag{6}$$

where p_0 denotes the signal power of the common stream and σ^2 is the noise. Once the common stream is successfully decoded, the k-th user can remove the common stream and treat other private streams as noise. The SINR of the k-th user decoding the private stream s_k is

$$\gamma_k^{private} = \frac{\left|\boldsymbol{h}_k^T\boldsymbol{w}_k p_k\right|^2}{\sum_{j\neq k}\left|\boldsymbol{h}_k^T\boldsymbol{w}_j p_j\right|^2 + \sigma^2}, j \in [1, N_r]. \tag{7}$$

Hence, with the increase of the number of users, each user performs SIC only once for common stream and then decodes the desired private stream considering other private streams as noise.

B. Precoding and power allocation constraints

A typical current-driven LED has a limited linear range [43] (see Fig. 3). Moreover, for an under-driven LED, either the LED cannot be turned on, or the LED cannot operate in the linear region. Adding the DC bias can guarantee the brightness of each LED luminary as well as the non-negative signal transmission. Conversely, for an over-driven LED, not only will the LED life-expectancy reduce, but also the self-heating effect will lead to a drop in the electrical-to-optical conversion efficiency.

Considering the precoding operation in (4), the data $\mathbf{W}\boldsymbol{s}$ at each LED have a constraint of

$$-\|\boldsymbol{\omega}_i\|_1 \leq \boldsymbol{s'}_i \leq \|\boldsymbol{\omega}_i\|_1, \tag{8}$$

where $\boldsymbol{\omega}_i^T$ is the row vector of $\mathbf{W}$, $\boldsymbol{s'} \triangleq \mathbf{W}\boldsymbol{s}$ and $\boldsymbol{s'}_i$ denote the i-th data row of $\mathbf{W}\boldsymbol{s}$. Note that the binary symbol $\{\pm 1\}$ is assumed for the transmitted symbol set of $\boldsymbol{s}$.

Considering the characteristics of the LEDs, the transmit signal of 1-layer RSMA at each LED should satisfy $\boldsymbol{I}_{\mathrm{L}} \leq \boldsymbol{x} \leq \boldsymbol{I}_U$, where $I_{\mathrm{U}} > I_{\mathrm{L}} > 0$ indicates the upper and lower bounds of the LED drive current within the linear region. Combining (8) and $\boldsymbol{I}_{\mathrm{L}} \leq \boldsymbol{x} \leq \boldsymbol{I}_U$ yields

$$\begin{matrix} I_{\mathrm{DC}} - \|\boldsymbol{\omega}_i\|_1 \geq I_{\mathrm{L}} \\ I_{\mathrm{DC}} + \|\boldsymbol{\omega}_i\|_1 \leq I_{\mathrm{U}} \end{matrix}, \tag{9}$$

where $\forall d_i = I_{DC}, d_i \in \boldsymbol{d}$. Hence, the constraint of the precoding matrix is presented in (10) to ensure that the LED operates within its dynamic range and avoid signal clipping.

$$\|\boldsymbol{\omega}_i\|_1 \leq \min\left(I_{\mathrm{DC}} - I_{\mathrm{L}}, I_{\mathrm{U}} - I_{\mathrm{DC}}\right) \tag{10}$$

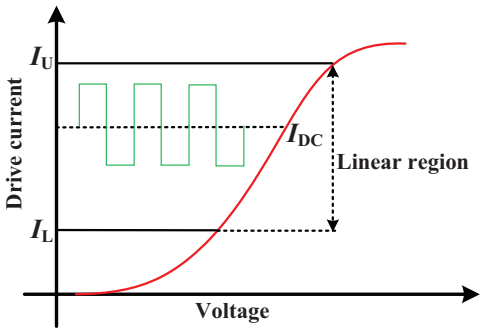

Fig. 3. Limited linear current range of LEDs.

Moreover, we define p_0 as the signal power of the total common stream, and p_k denotes the signal power of the corresponding private stream for the k-th user. Hence, considering the optical-electrical conversion, we can derive the constraint of the signal power allocation as follows:

$$p_0 + \sum_{k=1}^{N_r} p_k \leq P_t, \tag{11}$$

where P_t is the optical transmitted power.

C. Optimization model

The capacity of the IM/DD optical channel is yet unknown in closed-form expression [42]. However, when the input distribution of visible-light signals are modeled as truncated Gaussian or uniformly-spaced discrete distribution, in previous studies [44]–[48], bounding capacity of IM/DD optical channel have attained the achievable data rate in which the constant coefficients such as $\frac{e}{2\pi}$, $\frac{1}{2\pi e}$ and $\frac{2}{\pi e}$ are accompanied with signal-to-noise ratio (SNR) and SINR under different constraints. Considering that the certain constant coefficients have no influence on the following optimizing process, we indicate that the properties of numerical optimization in the mathematical form of the achievable data rate has the consistency of that in the Shannon's theorem.

Let us assume that c_k is the k-th user's portion of the common stream rate, and the number of all users is N_r. The data rate of the k-th user includes two parts, i.e., $R_{k,tot} = c_k + \log_2\left(1+\gamma_k^{private}\right), k \in [1, N_r]$. When we focus on the data rate of common stream, the achievable rate C_K in the whole common stream can be expressed as

$$\sum_{k=1}^{K} c_k = C_K = \min\left\{\log_2\left(1+\gamma_k^{common}\right), k \in [1, N_r]\right\}. \quad (12)$$

When we focus on the maximization of system spectral efficiency in $\max\limits_{\mathbf{W},\boldsymbol{p}} \sum\limits_{k=1}^{N_r} R_{k,tot}$, the optimization target and constraints are equivalently obtained as follows:

$$\max_{\mathbf{W},\boldsymbol{p}} C_K + \sum_{k=1}^{N_r} \log_2\left(1+\gamma_k^{private}\right) \quad (13a)$$

$$\text{s.t.} \quad \|\boldsymbol{\omega}_i\|_1 \le \min\left(I_{\mathrm{DC}} - I_{\mathrm{L}}, I_{\mathrm{U}} - I_{\mathrm{DC}}\right) \quad (13b)$$

$$\|\boldsymbol{p}\|_1 \le P_t \quad (13c)$$

$$\min\left(\boldsymbol{p}\right) \ge p_{\min} \cdot P_t \quad (13d)$$

$$\boldsymbol{h} \propto (1), \quad (13e)$$

where $\boldsymbol{p} = \left[p_0, p_1, \cdots, p_k, \cdots, p_{N_r}\right]$ and $p_{\min}$ are the minimum required power. Note that $\propto$ in (13e) indicates that $\boldsymbol{h}$ follows (1).

Because of the non-convexity of the original optimization problem, an interior point algorithm [49], [50] that combines trust region strategy and line search algorithm is selected by this study to solve the optimization problem; references [49], [50] prove that this interior point algorithm is modified to cope with non-convexity and possesses global convergence properties. Using the MATLAB-based convex optimization tool, we can introduce the programming function interface called '*fmincon*' which includes this interior point algorithm [49]–[51]. While transforming the target (13a) into $\min\limits_{\mathbf{W},\boldsymbol{p}} \frac{1}{\sum\limits_{k=1}^{N_r} R_{k,tot}}$, the function interface can be used to obtain the result of search convergence after a sufficient number of iterations.

IV. Simulations and Results

As indicated in Table I, we use the existing simulation parameters and their values as in [9], [40], [43]. As the optical attocell is very small [7], indoor VLC networks in the cramped space may limit the number of transmitters and receivers. Since the latticed deployment [14]–[16] is commonly used in multi-cell scenarios, it can be modelled as a basic unit including two LED arrays, where other lattices can be extended through the composition of the basic unit. In addition, considering multi-cell ICI and PD-NOMA, we selected the superposition coding (SC) at the transmitter and SIC at the receivers (denoted as SC-SIC) [22] as a NOMA benchmark scheme.

TABLE I
Parameters.

Symbol	Value	Symbol	Value
r_{oe}	0.53 (A/W)	Ψ_{FOV}	$60^\circ \sim 80^\circ$
$\Phi_{1/2}$	$60^\circ \sim 80^\circ$	LEDs per array	25
N_t	2 arrays	P_t	e.g. 1 (W) $\approx$ 30 (dBm)
T_f	1	n_{re}	1.5
A	$10^{-4}(\mathrm{m}^2)$	L	2.5 (m)
N_0	$10^{-21}(\mathrm{A}^2/\mathrm{Hz})$	B	20 (MHz)
I_{U}	1000 mA	I_{L}	200 mA
I_{DC}	600 mA	Room size	$10 \times 6 \times 3.5(\mathrm{m}^3)$
$p_{\min}$	0.1	N_r	$2 \sim 8$
LED array 1	$(3\mathrm{m}, 3\mathrm{m})$	LED array 2	$(7\mathrm{m}, 3\mathrm{m})$

The simulations are designed in two types. The first one is to observe the performance of spectral efficiency with varied transmitted power and number of users. The second one indicates the factors of user location and the influence of lighting deployment that affect the advantage of the 1-layer RSMA. The simulations were performed using Monte Carlo simulations to generate a uniform user distribution in local areas. Note that all users are covered by all LEDs, and the spectral efficiency in comparison is defined as the ratio of the system bit rate to the system bandwidth.

A. Spectral efficiency with varied transmitted power P_t and number of users N_r

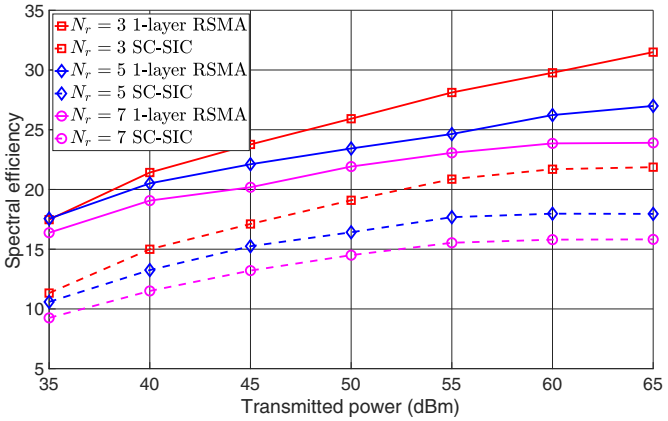

Fig. 4. Comparison of spectral efficiency for varied transmitted power P_t, when $\|\boldsymbol{\omega}_i\|_1 \le 0.4$ (A) with each LED.

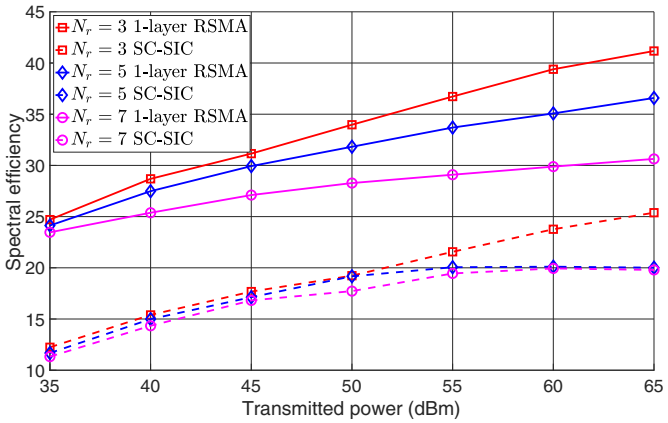

Fig. 5. Comparison of spectral efficiency for varied transmitted power P_t, when $\|\boldsymbol{\omega}_i\|_1 \leq 4$ (A) with each LED.

Fig. 4 shows that the average spectral efficiency is given by the mean value of spectral efficiency in the Monte Carlo simulations. As P_t increases, 1-layer RSMA outperforms the benchmark scheme. When N_r is small, the growth of the 1-layer RSMA is better than that of the benchmark. Among the different N_r cases, the increasing space between curves of spectral efficiency is clear in 1-layer RSMA.

When the transmitted power is high, 1-layer RSMA with a large number of users cannot guarantee the rise with a similar slope as shown in Fig. 4. For this behavior, we consider that the limitation of the LED effect might cause a loss of transmitted power. To further confirm this trend, the plot shown in Fig. 5 is obtained, wherein the current range of limited linear region is enlarged. In Fig. 5, when the number of users increases, 1-layer RSMA shows a clear increasing gradient, whereas the benchmark scheme has no significant improvement.

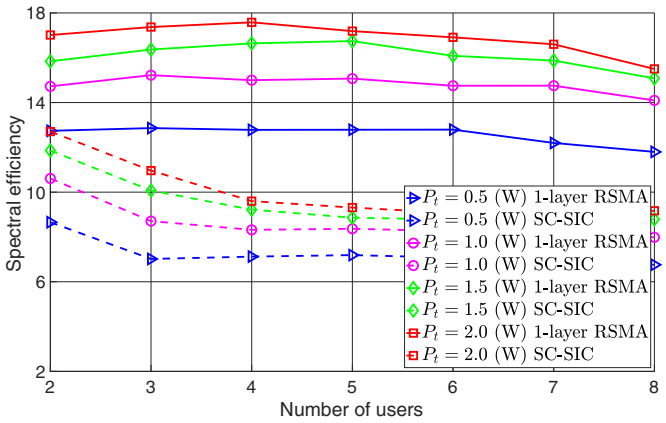

Fig. 6. Comparison of spectral efficiency for varied number of users, when $P_t = 0.5 \sim 2.0$ (W).

Compared to Figs. 4 and 5, Fig. 6 is based on a much smaller transmitted signal power and different number of users. In Fig. 6, with the increase of the number of users, 1-layer RSMA guarantees the stable system spectral efficiency, whereas the benchmark scheme fails to maintain it. Hence, the overall gain introduced by using the 1-layer RSMA from the system level is greater than the overall gain by using the benchmark scheme.

B. Advantages of 1-layer RSMA with varied locations and lighting deployment

Compared to traditional radio frequency, VLC cells possess a strong relationship with user locations and illumination. To better analyse the competitive advantages in visible light, we present the result of the simulations through Figs. 7, 8, and 9.

With respect to user locations, Fig. 7 was configured as follows. First, the location of a user is varied in the coverage of two LED arrays, while the locations of other users are fixed and labelled. Second, we evaluate the increment of spectral efficiency using 1-layer RSMA with respect to the benchmark scheme at ergodic locations of the complete room. The colours at the locations of the complete room indicate an increment in the worst case of spectral efficiency. Finally, the relationship between the advantages of the 1-layer RSMA and user locations can be observed.

On the one hand, the performance of the 1-layer RSMA is superior to that of the benchmark scheme. When the total number of users is 2, the user with a varied location tends to stay away from the fixed user, which can introduce significant increment in spectral efficiency. On the other hand, the locations with the advantage of where 1-layer RSMA is superior to the benchmark scheme have a symmetry. This result suggests that the symmetry is involved with visible-light channels. In IM/DD, due to intensity modulation without phase, the visible-light channel gain model in Lambertian radiation primarily indicates an intensity change and a strong correlation with the direction angle and distance from targeted users.

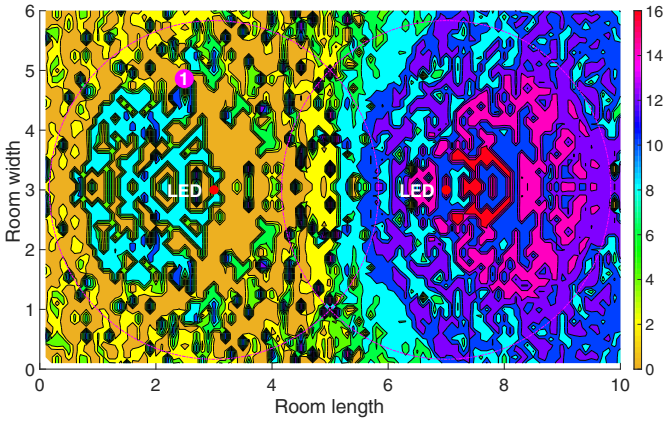

Fig. 7. Spectral efficiency comparisons with one user in varied locations and one fixed user (when the total number of users is 2).

Furthermore, when a user standing at the symmedian point receives two optical links, the user practically has similar channel gains from two directions of two LED arrays which are at the same distances. Hence, the symmedian point in left-right symmetrical direction reveals a strong ICI. For the

symmedian point in the overlapping area of two cells, 1-layer RSMA guarantees the advantage.

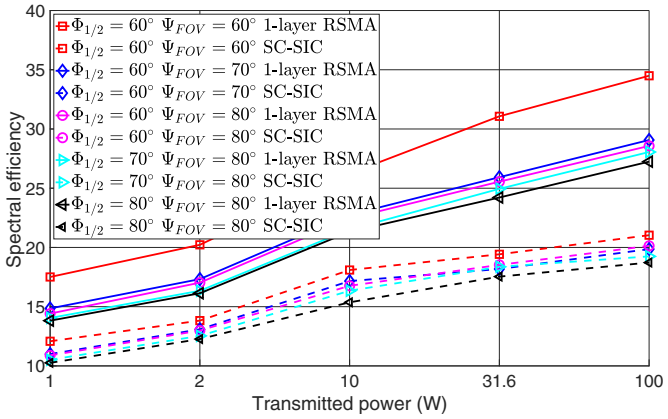

Fig. 8. Spectral efficiency comparisons with varied P_t, $\Phi_{1/2}$ and Ψ_{FOV}, when $N_r = 2$.

In VLC, lighting deployment, including half-power semi-angle (i.e., $\Phi_{1/2}$) at the transmitter and FOV (i.e., Ψ_{FOV}) at a receiver, is one part of the cell deployment. Note that the aforementioned simulations are based on $\Phi_{1/2} = 60^\circ$ and $\Psi_{FOV} = 80^\circ$. Based on the same parameters listed in Table 1, except $\Phi_{1/2}$ and Ψ_{FOV}, Figs. 8 and 9 are obtained by the varied $\Phi_{1/2}$ and Ψ_{FOV} to observe the influence of light angles on both 1-layer RSMA and benchmark strategies with multiple users.

In Fig. 8, when $\Phi_{1/2}$ is fixed, a decrease in Ψ_{FOV} conveys an increase in spectral efficiency. Compared with the benchmark scheme, 1-layer RSMA results shows a clear enhancement, which implies that the spectral efficiency in the benchmark scheme lacks sufficient climbing space. As shown in Fig. 1, FOV indicates the acceptable threshold for the received angle and controls of the receiver coverage. When FOV is larger, a user standing in the overlapping area of two LED arrays receives signals from more directional angles, leading to an easy reception of more inter-cell channel interference.

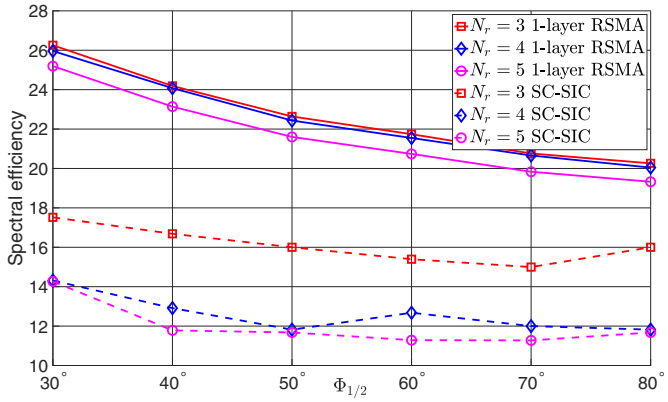

Fig. 9. Spectral efficiency comparisons with varied $\Phi_{1/2}$ and N_r, when $\Psi_{FOV} = 80^\circ$ and $P_t = 10$ (W).

In Fig. 8, when Ψ_{FOV} is fixed, the decrease in $\Phi_{1/2}$ reflects the unclear rise in spectral efficiency. To further confirm the details, we generate the plots in Fig. 9 with fixed Ψ_{FOV} and varied $\Phi_{1/2}$. First, compared with the adjustment of Ψ_{FOV} and fixed $\Phi_{1/2}$, varied $\Phi_{1/2}$ with fixed Ψ_{FOV} has a degree of enhancement of spectral efficiency. Second, compared to the benchmark scheme, 1-layer RSMA has a marked increase in the performance with the decrease of $\Phi_{1/2}$.

In summary, the noticeable improvement can be attributed to adjusting FOV. As the lighting deployment is adjusted, the aggregate spectral efficiency is improved in 1-layer RSMA, whereas in the benchmark scheme it is not.

V. Conclusion

To solve the ICI problems, we introduced the RSMA into indoor multi-cell VLC networks. Based on the Lambertian radiation model of visible-light channels, we investigated the advantages of spectral efficiency in 1-layer RSMA, which is combined with the specific constraints of optical signals and the LED effect. From numerical simulations, we discovered that the advantages of 1-layer RSMA with the Lambertian model are involved with the user locations. Additionally, 1-layer RSMA can guarantee the advantage of system spectral efficiency compared with the benchmark of PD-NOMA. In future, we will focus on the spectral efficiency analysis with analytic forms in RSMA-VLC and investigate the lighting deployment with RSMA.

Acknowledgment

This work was supported by the National Natural Science Foundation of China (No. 61601516 and No. 61671477). Doctor Siyu Tao appreciates the valuable suggestions and technical support of Dr. Yijie Mao, Dr. Di Zhang, and Dr. Jianping Du.

References

[1] S. Wu, H. Wang, and C.-H. Youn, "Visible light communications for 5G wireless networking systems: from fixed to mobile communications," *IEEE Netw.*, vol. 28, no. 6, pp. 41–45, Nov. 2014.

[2] Q. Wang, Z. Wang, and L. Dai, "Multiuser MIMO-OFDM for visible light communications," *IEEE Photon. J.*, vol. 7, no. 6, pp. 1–11, Dec. 2015.

[3] H. Marshoud, V. M. Kapinas, G. K. Karagiannidis, and S. Muhaidat, "Non-orthogonal multiple access for visible light communications," *IEEE Photon. Technol. Lett.*, vol. 28, no. 1, pp. 51–54, Jan. 2016.

[4] F. Yang, J. Gao, and S. Liu, "Novel visible light communication approach based on hybrid OOK and ACO-OFDM," *IEEE Photon. Technol. Lett.*, vol. 28, no. 14, pp. 1585–1588, July 2016.

[5] Q. Wang, Z. Wang, and L. Dai, "Asymmetrical hybrid optical OFDM for visible light communications with dimming control," *IEEE Photon. Technol. Lett.*, vol. 27, no. 9, pp. 974–977, May 2015.

[6] C.-X. Wang, F. Haider, X. Gao, X.-H. You, Y. Yang, D. Yuan, H. M. Aggoune, H. Haas, S. Fletcher, and E. Hepsaydir, "Cellular architecture and key technologies for 5G wireless communication networks," *IEEE Commun. Mag.*, vol. 52, no. 2, pp. 122–130, Feb. 2014.

[7] H. Haas, L. Yin, Y. Wang, and C. Chen, "What is lifi?" *Journal of Lightwave Technology*, vol. 34, no. 6, pp. 1533–1544, Mar. 2015.

[8] D. Zhang, Y. Liu, L. Dai, A. K. Bashir, A. Nallanathan, and B. Shim, "Performance analysis of FD-NOMA-based decentralized V2X systems," *IEEE Trans. Commun.*, vol. 67, no. 7, pp. 5024–5036, July 2019.

[9] L. Yin, W. O. Popoola, X. Wu, and H. Haas, "Performance evaluation of non-orthogonal multiple access in visible light communication," *IEEE Trans. Commun.*, vol. 64, no. 12, pp. 5162–5175, Dec. 2016.

[10] H. Marshoud, S. Muhaidat, P. C. Sofotasios, S. Hussain, M. A. Imran, and B. S. Sharif, "Optical non-orthogonal multiple access for visible light communication," *IEEE Wireless Commun.*, vol. 25, no. 2, pp. 82–88, Apr. 2018.

[11] M. Moltafet, N. Mokari, M. R. Javan, H. Saeedi, and H. Pishro-Nik, "A new multiple access technique for 5G: power domain sparse code multiple access (PSMA)," *IEEE Access*, vol. 6, pp. 747–759, Nov. 2017.

[12] C. Chen, W.-D. Zhong, H. Yang, P. Du, and Y. Yang, "Flexible-rate SIC-free NOMA for downlink VLC based on constellation partitioning coding," *IEEE Wireless Commun. Lett.*, vol. 8, no. 2, pp. 568–571, Apr. 2018.

[13] H. Li, Z. Huang, Y. Xiao, S. Zhan, and Y. Ji, "A power and spectrum efficient NOMA scheme for VLC network based on hierarchical predistorted LACO-OFDM," *IEEE Access*, vol. 7, pp. 48 565–48 571, Apr. 2019.

[14] X. Zhang, Q. Gao, C. Gong, and Z. Xu, "User grouping and power allocation for NOMA visible light communication multi-cell networks," *IEEE Commun. Lett.*, vol. 21, no. 4, pp. 777–780, Apr. 2017.

[15] Z. Yang, W. Xu, and Y. Li, "Fair non-orthogonal multiple access for visible light communication downlinks," *IEEE Wireless Commun. Lett.*, vol. 6, no. 1, pp. 66–69, Feb. 2017.

[16] X. Guan, Q. Yang, and C.-K. Chan, "Joint detection of visible light communication signals under non-orthogonal multiple access," *IEEE Photon. Technol. Lett.*, vol. 29, no. 4, pp. 377–380, Feb. 2017.

[17] R. Mitra and V. Bhatia, "Chebyshev polynomial-based adaptive predistorter for nonlinear LED compensation in VLC," *IEEE Photon. Technol. Lett.*, vol. 28, no. 10, pp. 1053–1056, May 2016.

[18] C. Chen, W.-D. Zhong, H. Yang, and P. Du, "On the performance of MIMO-NOMA-based visible light communication systems," *IEEE Photon. Technol. Lett.*, vol. 30, no. 4, pp. 307–310, Feb. 2018.

[19] B. Lin, Z. Ghassemlooy, X. Tang, Y. Li, and M. Zhang, "Experimental demonstration of optical MIMO NOMA-VLC with single carrier transmission," *Optics Communications*, vol. 402, pp. 52–55, Nov. 2017.

[20] X. Guan, Y. Hong, and C. C.-K. Chan, "Non-orthogonal multiple access with multicarrier precoding in visible light communications," in *2016 21st OptoElectronics and Communications Conference (OECC)*. IEEE, July 2016, pp. 1–3.

[21] W. Shin, M. Vaezi, B. Lee, D. J. Love, J. Lee, and H. V. Poor, "Non-orthogonal multiple access in multi-cell networks: theory, performance, and practical challenges," *IEEE Commun. Mag.*, vol. 55, no. 10, pp. 176–183, Oct. 2017.

[22] Y. Mao, B. Clerckx, and V. O. Li, "Rate-splitting multiple access for downlink communication systems: bridging, generalizing, and outperforming SDMA and NOMA," *EURASIP Journal on Wireless Communications and Networking*, vol. 2018, no. 133, pp. 1–54, May 2018.

[23] ——, "Rate-splitting for multi-antenna non-orthogonal unicast and multicast transmission: spectral and energy efficiency analysis," *IEEE Trans. Commun.*, vol. 67, no. 12, pp. 8754–8770, Sept. 2019.

[24] Y. Mao and B. Clerckx, "Beyond dirty paper coding for multi-antenna broadcast channel with partial CSIT: A rate-splitting approach," *arXiv preprint arXiv:1912.05409*, 2019.

[25] Y. Mao, B. Clerckx, J. Zhang, V. O. Li, and M. Arafah, "Max-min fairness of K-user cooperative rate-splitting in MISO broadcast channel with user relaying," *arXiv preprint arXiv:1910.07843*, 2019.

[26] H. Joudeh and B. Clerckx, "Sum-rate maximization for linearly precoded downlink multiuser MISO systems with partial CSIT: A rate-splitting approach," *IEEE Trans. Commun.*, vol. 64, no. 11, pp. 4847–4861, Nov. 2016.

[27] ——, "Robust transmission in downlink multiuser MISO systems: A rate-splitting approach," *IEEE Trans. Signal Process.*, vol. 64, no. 23, pp. 6227–6242, Dec. 2016.

[28] M. Medra and T. N. Davidson, "Robust downlink transmission: An offset-based single-rate-splitting approach," in *2018 IEEE 19th Int. Workshop on Signal Process. Advances in Wireless Commun. (SPAWC)*. IEEE, June 2018, pp. 1–5.

[29] Y. Mao, B. Clerckx, and V. O. Li, "Energy efficiency of rate-splitting multiple access, and performance benefits over SDMA and NOMA," in *2018 15th Int. Symposium on Wireless Commun. Systems (ISWCS)*. IEEE, Aug. 2018, pp. 1–5.

[30] M. Dai, B. Clerckx, D. Gesbert, and G. Caire, "A rate splitting strategy for massive MIMO with imperfect CSIT," *IEEE Trans. Wireless Commun.*, vol. 15, no. 7, pp. 4611–4624, July 2016.

[31] A. Papazafeiropoulos, B. Clerckx, and T. Ratnarajah, "Rate-splitting to mitigate residual transceiver hardware impairments in massive MIMO systems," *IEEE Trans. Veh. Technol.*, vol. 66, no. 9, pp. 8196–8211, Sept. 2017.

[32] M. Dai and B. Clerckx, "Multiuser millimeter wave beamforming strategies with quantized and statistical CSIT," *IEEE Trans. Wireless Commun.*, vol. 16, no. 11, pp. 7025–7038, Nov. 2017.

[33] O. Kolawole, A. Panazafeironoulos, and T. Ratnarajah, "A rate-splitting strategy for multi-user millimeter-wave systems with imperfect CSI," in *2018 IEEE 19th Int. Workshop on Signal Process. Advances in Wireless Commun. (SPAWC)*. IEEE, June 2018, pp. 1–5.

[34] H. Joudeh and B. Clerckx, "Sum rate maximization for MU-MISO with partial CSIT using joint multicasting and broadcasting," in *2015 IEEE Int. Conf. on Commun. (ICC)*. IEEE, June 2015, pp. 4733–4738.

[35] O. Tervo, L.-N. Trant, S. Chatzinotas, B. Ottersten, and M. Juntti, "Multigroup multicast beamforming and antenna selection with rate-splitting in multicell systems," in *2018 IEEE 19th Int. Workshop on Signal Process. Advances in Wireless Commun. (SPAWC)*. IEEE, June 2018, pp. 1–5.

[36] Y. Mao, B. Clerckx, and V. O. Li, "Rate-splitting multiple access for coordinated multi-point joint transmission," in *2019 IEEE Int. Conf. on Commun. Workshops (ICC Workshops)*. IEEE, May 2019, pp. 1–6.

[37] A. A. Ahmad, H. Dahrouj, A. Chaaban, A. Sezgin, and M.-S. Alouini, "Interference mitigation via rate-splitting in cloud radio access networks," in *2018 IEEE 19th Int. Workshop on Signal Process. Advances in Wireless Commun.(SPAWC)*. IEEE, June 2018, pp. 1–5.

[38] Y. Mao, B. Clerckx, and V. O. Li, "Rate-splitting for multi-user multi-antenna wireless information and power transfer," in *2019 IEEE 20th Int. Workshop on Signal Process. Advances in Wireless Commun. (SPAWC)*. IEEE, July 2019, pp. 1–5.

[39] J. Zhang, B. Clerckx, J. Ge, and Y. Mao, "Cooperative rate splitting for MISO broadcast channel with user relaying, and performance benefits over cooperative NOMA," *IEEE Signal Process. Lett.*, vol. 26, no. 11, pp. 1678–1682, Nov. 2019.

[40] T. Komine and M. Nakagawa, "Fundamental analysis for visible-light communication system using LED lights," *IEEE Trans. Consum. Electron.*, vol. 50, no. 1, pp. 100–107, June 2004.

[41] L. Hua, Y. Zhuang, L. Qi, J. Yang, and L. Shi, "Noise analysis and modeling in visible light communication using Allan variance," *IEEE Access*, vol. 6, pp. 74 320–74 327, Dec. 2018.

[42] R. Jiang, Q. Wang, H. Haas, and Z. Wang, "Joint user association and power allocation for cell-free visible light communication networks," *IEEE J. Sel. Areas Commun.*, vol. 36, no. 1, pp. 136–148, Jan. 2018.

[43] Z.-G. Sun, H.-Y. Yu, Z.-J. Tian, and Y.-J. Zhu, "Linear precoding for MU-MISO VLC systems with noisy channel state information," *IEEE Commun. Lett.*, vol. 22, no. 4, pp. 732–735, Jan. 2018.

[44] J. Zhou and W. Zhang, "Bounds on the capacity region of the optical intensity multiple access channel," *IEEE Trans. Commun.*, vol. 67, no. 11, pp. 7629–7641, Nov. 2019.

[45] A. Lapidoth, S. M. Moser, and M. A. Wigger, "On the capacity of free-space optical intensity channels," *IEEE Trans. on Inf. Theory*, vol. 55, no. 10, pp. 4449–4461, Oct. 2009.

[46] A. Chaaban, J.-M. Morvan, and M.-S. Alouini, "Free-space optical communications: Capacity bounds, approximations, and a new sphere-packing perspective," *IEEE Trans. Commun.*, vol. 64, no. 3, pp. 1176–1191, Mar. 2016.

[47] H. Shen, Y. Deng, W. Xu, and C. Zhao, "Rate maximization for downlink multiuser visible light communications," *IEEE Access*, vol. 4, pp. 6567–6573, Sept. 2016.

[48] H. Shen, Y. Wu, W. Xu, and C. Zhao, "Optimal power allocation for downlink two-user non-orthogonal multiple access in visible light communication," *Journal of Communications and Information Networks*, vol. 2, no. 4, pp. 57–64, Dec. 2017.

[49] R. H. Byrd, M. E. Hribar, and J. Nocedal, "An interior point algorithm for large-scale nonlinear programming," *SIAM Journal on Optimization*, vol. 9, no. 4, pp. 877–900, 1999.

[50] R. A. Waltz, J. L. Morales, J. Nocedal, and D. Orban, "An interior algorithm for nonlinear optimization that combines line search and trust region steps," *Mathematical programming*, vol. 107, no. 3, pp. 391–408, Nov. 2005.

[51] MathWorks Inc. Constrained nonlinear optimization algorithms. [Online]. Available: http://www.mathworks.com/help/optim/ug/constrained-nonlinear-optimization-algorithms.html